Improvement in Fatigue Strength of Biomedical β-type Ti–Nb–Ta–Zr Alloy While Maintaining Low Young's Modulus Through Optimizing ω-Phase Precipitation

MASAAKI NAKAI, MITSUO NIINOMI, and TAKAHIRO ONEDA

The improvement in fatigue strength, with maintenance of a low Young's modulus, in a biomedical β-type titanium alloy, Ti–29Nb–13Ta–4.6Zr (TNTZ), by thermomechanical treatment was investigated. A short aging time at an ω-phase-forming temperature combined with severe cold rolling was employed. A fine ω phase is observed in TNTZ subjected to this thermomechanical treatment. Because the rolling texture of β phase is formed by cold rolling, such as the ω phase may be preferentially oriented to a direction that is effective for inhibiting the increase in Young's modulus. The samples aged at 573 K (300 °C) for 3.6 ks and 10.8 ks after cold rolling exhibit a good balance between a high tensile strength and low Young's modulus. In the case of the sample aged for 3.6 ks, the tensile strength is improved, although the fatigue strength is not improved significantly. Both the tensile strength and the fatigue strength of the sample aged for 10.8 ks are improved. This fatigue strength is the highest among the TNTZ samples used in the current and in previous studies with Young's moduli less than 80 GPa.

I. INTRODUCTION

MECHANICAL biocompatibility is required in titanium alloys for biomedical applications where the alloy is used as a substitute for human hard tissues.[1] These titanium alloys should possess a low Young's modulus, similar to that of cortical bone (10−30 GPa[2,3]) to prevent stress-shielding effects[4] but must maintain mechanical properties such as high fatigue strength. A biomedical β-type titanium alloy, Ti–29Nb–13Ta–4.6Zr (TNTZ), which exhibits a low Young's modulus of approximately 60 GPa after solution treatment, has been developed by the authors.[5] Various thermomechanical treatments have been examined for improving the fatigue strength of TNTZ[6–11] because its fatigue strength after solution treatment is lower than that of Ti–6Al–4V ELI (Ti64), which is a titanium alloy currently used for biomedical applications. Our previous studies showed that the fatigue strength of TNTZ can be improved to the same level as that of Ti64 by certain thermomechanical treatments; for example, TNTZ subjected to aging at 723 K (450 °C) for 259.2 ks after cold rolling with a reduction ratio of approximately 90 pct exhibited a high fatigue strength of approximately 780 MPa.[8,9] In this case, a fine, dense α phase was precipitated during aging as a result of the high density

of dislocations introduced during cold rolling before aging; significant precipitation strengthening occurred because of the α phase. However, a large amount of α phase was precipitated during the aging treatment, resulting in a large increase in the Young's modulus, to above 80 GPa, and thus a loss of the excellent features of TNTZ. Previous attempts have been made to improve the fatigue strength of TNTZ without increasing the Young's modulus using work hardening by cold rolling.[9] In this case, the tensile strength increased and the Young's modulus did not increase, as expected, but the fatigue strength could not be increased by cold rolling. Until now, precipitation strengthening has been the only useful method for improving the fatigue strength of TNTZ. The amount of precipitate formed is likely to be decreased by shortening the aging time. Optimization of the aging time to control precipitation is an effective approach to maintaining a low Young's modulus; however, a low level of precipitation may reduce the precipitation strengthening. In this case, the ω phase is considered to be appropriate because it can sometimes produce a larger increase in the tensile strength than that produced by the α phase, although too much ω-phase precipitation decreases ductility drastically.[6–9] Furthermore, to inhibit the increase in Young's modulus because of the ω-phase precipitation, the texture of β matrix should be considered because the ω phase is usually formed with a certain orientation relationship with β matrix,[12] and the Young's moduli of crystalline materials generally depend on their crystallographic orientations.[13] Precipitation of the ω phase in TNTZ subjected to aging treatments at 573 K (300 °C)[6,7,10,11] or 598 K (325 °C)[6–9] has been observed. On the basis of these results, aging treatments after cold rolling were examined at 573 K (300 °C) for

MASAAKI NAKAI, Associate Professor, and MITSUO NIINOMI, Professor, are with the Institute for Materials Research, Tohoku University, Sendai 980-8577, Japan. Contact e-mail: nakai@imr.tohoku.ac.jp TAKAHIRO ONEDA, Graduate Student, formerly with the Department of Materials Science, Graduate School of Engineering, Tohoku University, is now with NGK Insulators, Ltd., Nagoya 467-8530, Japan.

short periods of up to 86.4 ks. The thermomechanical treatment for obtaining TNTZ having both a low Young's modulus and high fatigue strength was optimized in this study.

II. EXPERIMENTAL PROCEDURES

A. *Material*

Figure 1 shows the schematic drawing of the thermomechanical treatment employed in this study. A hot-forged bar of TNTZ (Ti: balance, Nb: 30.0, Ta: 13.5, Zr: 4.72, O: 0.071, C: 0.006, N: 0.009 mass pct) with a diameter of approximately 25 mm was cut to a length of approximately 50 mm and subjected to solution treatment in vacuum at 1063 K (790 °C) for 3.6 ks, followed by ice-water quenching (ST). After solution treatment, equiaxial grains with diameters of approximately 20 μm could be observed by optical microscopy. The ST sample was machined to a thickness of approximately 15 mm and cold rolled into a plate with a thickness of 2 mm (reduction ratio of 87 pct) at room temperature in air (CR). The CR samples were subjected to aging treatments at 573 K (300 °C) for 0.6, 1.8, 2.7, 3.6, 5.4, 10.8, 43.2, and 86.4 ks in vacuum, followed by ice-water quenching (AT0.6, AT1.8, AT2.7, AT3.6, AT5.4, AT10.8, AT43.2, and AT86.4, respectively).

B. *Microstructural Evaluation*

The microstructures of the samples were evaluated by X-ray diffraction analysis (XRD) and transmission electron microscopy (TEM). For XRD, the samples were cut into specimens with dimensions of 20 mm × 18 mm × 2 mm. The surfaces of the specimens were wet polished using emery papers of up to 4000 grit. XRD was carried out on the rolling plane in a scanning angle range of 30 deg to 90 deg at a scanning rate of 1 deg min^{-1} with Cu-Kα radiation at a voltage of 120 kV and a current of 40 mA. For TEM, the samples were cut into specimens with dimensions of 2 mm × 2 mm × 0.75 mm. The thickness of the specimens was reduced to 0.04 mm by wet polishing using emery papers of up to 4000 grit and buff polishing with Al$_2$O$_3$ powder. The thinned specimens were dimple ground to a thickness of 0.01 mm and thinned even more by ion
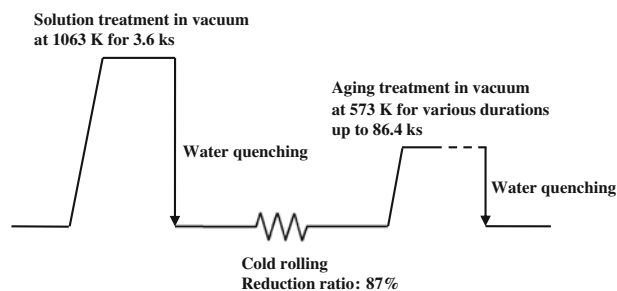
milling. TEM was carried out at an acceleration voltage of 200 kV.

C. *Mechanical Evaluation*

The Vickers hardness, Young's modulus, and tensile and fatigue properties were evaluated in this study. For the Vickers hardness tests, the samples were cut into specimens with dimensions of 20 mm × 18 mm × 2 mm. The surfaces of the specimens were wet polished using emery papers of up to 1500 grit. The hardness was measured on a rolling plane under a load of 980 mN for a holding time of 15 seconds.

The Young's moduli of the samples were measured by a free resonance method. For these measurements, the samples were cut into specimens with dimensions of 6 mm × 60 mm × 2 mm. Their longitudinal direction was set to be parallel to the rolling direction; the Young's modulus, measured in this study, corresponds to that of the sample with the axis parallel to rolling direction. Finally, the surfaces of the specimens were wet polished using emery papers of up to 1500 grit.

Tensile specimens with a cross-section of 3 mm × 1.5 mm and a gauge length of 13 mm were prepared from the samples by electrical discharge machining. Their longitudinal direction was also parallel to the rolling direction. The surfaces of the tensile specimens were wet polished using emery papers of up to 1500 grit. The tensile tests were carried out using an Instron-type machine with a cross-head speed of 8.33×10^{-6} m second^{-1} in air at room temperature. The load and strain were measured using a load cell attached to the machine, and a foil-type strain gauge attached to the gauge section of the specimens, respectively. The tensile strength and 0.2 pct proof stress were obtained from the tensile stress–strain curve. The elongation was obtained by measuring the gauge length of the specimens before and after the tensile tests.

Fatigue specimens with same geometry as the tensile specimens were prepared by electrical discharge machining. The surfaces of the fatigue specimens were wet polished using emery papers of up to 4000 grit and buff polished with Al$_2$O$_3$ powder and a SiO$_2$ suspension. The fatigue tests were carried out using an electroservohydraulic machine at a frequency of 10 Hz and a stress ratio of $R = 0.1$ in the tension–tension mode in air at room temperature. In this study, the fatigue limit was defined as the maximum cyclic stress, *i.e.*, the stress at which the specimens had still not failed after 10^7 cycles. After the fatigue tests, the fractured surfaces were observed by scanning electron microscopy (SEM).

III. RESULTS AND DISCUSSION

A. *Microstructure*

Figure 2 shows the XRD profiles obtained from the rolling planes of the ST, CR, and AT samples. Only the β-phase diffraction peaks are detected in every sample. According to our previous study, the ω phase appears in

Solution treatment in vacuum
at 1063 K for 3.6 ks

Water quenching

Aging treatment in vacuum
at 573 K for various durations
up to 86.4 ks

Water quenching

Cold rolling
Reduction ratio: 87%

Fig. 1—Schematic drawing of thermomechanical treatment for TNTZ employed in this study.

TNTZ after aging treatment at 573 K (300 °C) for 259.2 ks.[6,7] However, in this study, the ω phase cannot be identified clearly by XRD, even for the AT86.4 sample. This result indicates that the size and volume fraction of the ω phase are smaller than those pre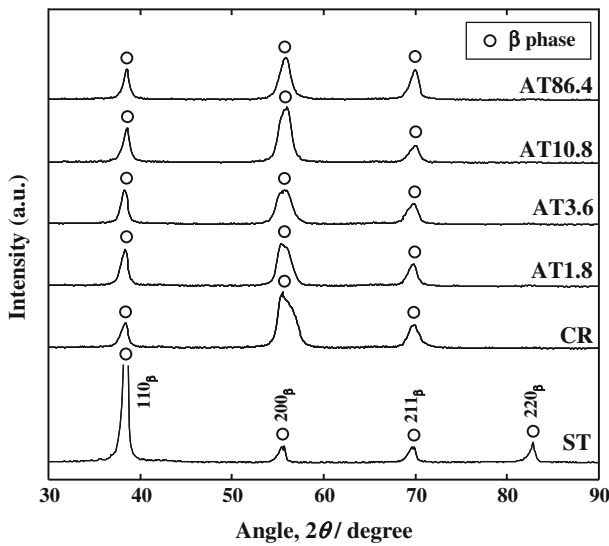cipitated in the previous study because of the short aging time. With regard to the β-phase peak intensities, the $(110)_\beta$ peak is the strongest among the β planes in the ST sample, but the $(200)_\beta$ peaks are stronger than the $(110)_\beta$ peaks in the CR and AT samples. Furthermore, the $(211)_\beta$ peaks in the CR and AT samples are slightly stronger than that in the ST sample. These results indicate that the texture is changed by cold rolling; the common rolling textures of strong $\{001\}_\beta\langle110\rangle_\beta$ and weak $\{211\}_\beta\langle110\rangle_\beta$ for body-centered-cubic (bcc) metals were probably formed by cold rolling and were not changed significantly by the subsequent aging treatment.

Figure 3 shows representative dark-field images and electron diffraction patterns of the CR and AT samples, obtained by TEM. The bcc lattice in TNTZ is unstable, and thus the microstructure of TNTZ is sensitive to chemical composition; the α'' phase is sometimes detected after water quenching in solution treatments[14,15] and after cold deformation[16,17] when the amounts of β-phase-stabilizing elements such as Nb and Ta become slightly lower than those in the intended composition. However, in the electron diffraction patterns of the CR sample, only the reflection from the β phase is obtained. The CR sample, therefore, comprises a single β phase. In contrast, the other reflection in addition to that of the β phase is obtained in the AT samples, and a fine second phase is observed in their dark-field images. The diffraction pattern analyses reveal that the ω phase having a common orientation relationship with β phase, $[111]_\beta // [0001]_\omega$,[12] is present

Fig. 2—XRD profiles obtained from rolling planes of ST, CR, and AT samples.
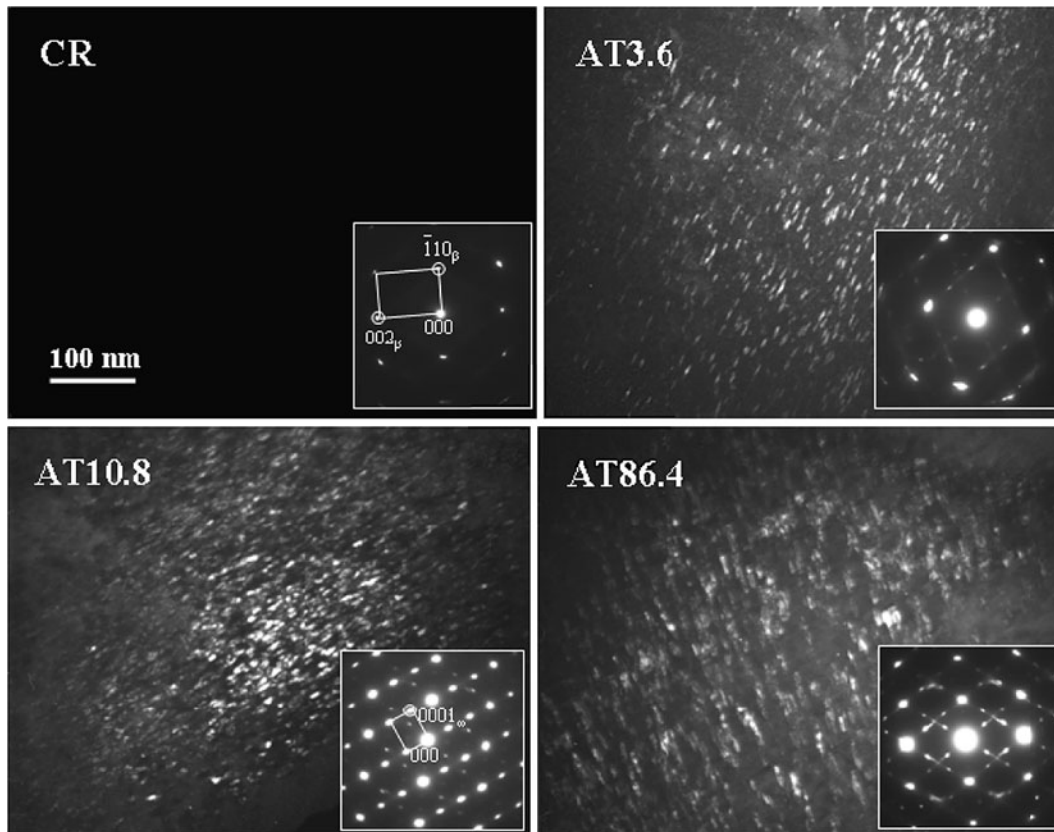

Fig. 3—Representative TEM micrographs of dark-field images and electron diffraction patterns of CR and AT samples. Beam direction is parallel to $[110]_\beta$.

in addition to the β phase. Furthermore, it is found that the reflection from a certain variant of the ω phase is stronger than that from another one in the AT3.6 and AT10.8 samples. This result implies that a preferred variant selection occurs at the early stage of ω-phase precipitation in cold-rolled TNTZ. The ω phase formed in β-type titanium alloys is sometimes difficult to be detected by XRD, but it can be observed by TEM when its size and volume fraction are small. The size and volume fraction of the ω phase precipitated in this study were small because of the short aging time. Therefore, it is considered that the detection of ω phase was limited by only TEM in this study.

B. Mechanical Properties

Figure 4 shows the Vickers hardness values of the ST, CR, and AT samples; the values indicate age hardening at 573 K (300 °C) for cold-rolled TNTZ. The lowest hardness is obtained for the ST sample. The Vickers hardness increases slightly with cold rolling as a result of work hardening. The Vickers hardness is not changed by aging treatments of up to 0.6 ks. For aging periods longer than 0.6 ks, the hardness increases monotonically with increasing aging time. It has been reported that the Vickers hardness is increased by ω-phase precipitation in TNTZ.[7,8,10,11] The ω phase therefore probably starts to precipitate in cold-rolled TNTZ for aging times longer than 0.6 ks.

Figure 5 shows the Young's moduli of the ST, CR, and AT samples. The pattern of changes in the Young's moduli is a little different from that for the Vickers hardness; the Young's modulus is decreased slightly by cold rolling and decreases even more with aging treatment for up to 0.6 ks. After 0.6 ks, the Young's modulus increases with increasing aging time.

It has been reported that the Young's modulus in TNTZ comprising a single β phase is strongly anisotropic and depends on the crystallographic orientation.[18] The XRD results indicated that the rolling textures of the β phase were observed after cold rolling. The slight decrease in the Young's modulus caused by

cold rolling may therefore be caused by the formation of rolling textures of β phase. Although the aging treatment did not drastically change the texture, Young's modulus decreased for aging times up to 0.6 ks. According to the literature, Young's modulus decreases around the temperature at which martensitic transformation starts, i.e., the Ms temperature in metastable β-type Ti–Nb-based alloys.[19,20] This phenomenon is considered to be related to a pretransition from the β phase to the α'' phase; the β-phase stability decreases before the martensitic transformation to the α'' phase, leading to a decrease in the Young's moduli of the β phase.[19,20] It is thought that a similar phenomenon may occur as a pretransitional phenomenon when ω-phase formation starts in TNTZ. As mentioned previously, ω-phase precipitation is considered to start for aging times longer than 0.6 ks. The β-phase-stabilizing elements such as Nb and Ta are released from the ω phase as well as the α phase via atomic diffusion during aging treatment in TNTZ.[21] Such atomic diffusion is considered to occur also during embryo formation before ω-phase nucleation. Therefore, the Nb- and/or Ta-depleted zones may be formed by the embryo formation at the early stage of aging treatment for up to 0.6 ks. In these zones, β-phase stability may decrease just before ω-phase nucleation, which results in a decrease in the Young's modulus of β phase.

In contrast, the increase in Young's modulus with increasing aging time beyond 0.6 ks is considered to correspond to the increase in the amount of ω phase. However, the Young's moduli of the samples aged for up to 3.6 ks are still lower than or almost equal to that of the ST sample even though the ω phase has already formed (Figure 3). This result is considered to be related to the amount of ω phase and its crystallographic orientation. According to the TEM results (Figure 3), one ω-phase variant was formed preferentially in the AT3.6 and AT10.8 samples, but another variant was formed additionally in the AT86.4 sample. This result implies that the amount of ω phase in the AT3.6 and AT10.8 samples is smaller than that in the AT86.4
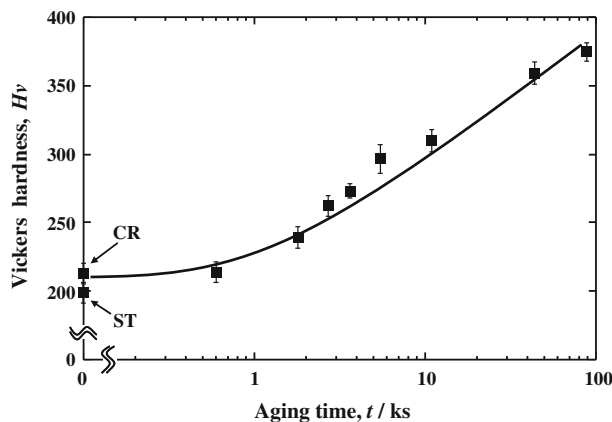

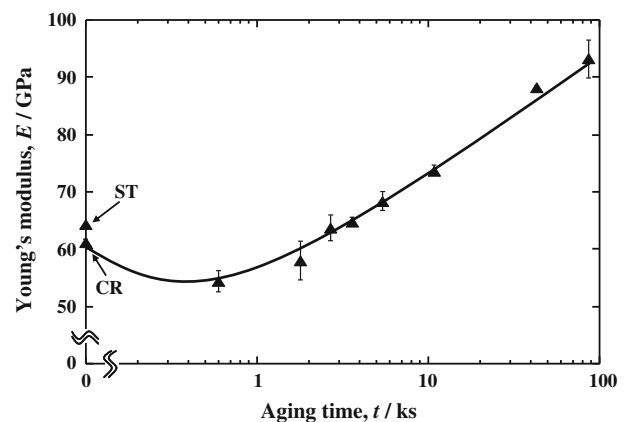Fig. 4—Vickers hardness values of ST, CR, and AT samples as a function of aging time.

Fig. 5—Young's moduli of ST, CR, and AT samples as a function of aging time.

sample. Moreover, the elastic stiffness constants of titanium comprising a single ω phase with hexagonal lattice (ω-Ti), C_{ij}, which were obtained by a first principle calculation, have been reported, whereas the calculated C_{ij} values correspond to those at 0 K (-273 °C).[22] The experimentally measured C_{ij} values are difficult to be obtained because titanium stabilizes in α phase with hexagonal close-packed (hcp) structure at ambient conditions and can transform into ω phase only at limited conditions at room temperature under high pressure.[23] However, it is believed that the calculated C_{ij} values for the ω phase are available to predict the Young's modulus because the reasonability of calculated C_{ij} values was confirmed by comparing the experimentally measured C_{ij} values using α phase. Therefore, to estimate the dependence of Young's modulus on the crystallographic orientation of ω phase, the calculated C_{ij} values are employed in this study. Because of the symmetry of hexagonal lattice, ω-Ti has the independent 5 C_{ij} (C_{11}, C_{12}, C_{13}, C_{33}, and C_{44}) and C_{66} can be obtained as

$$C_{66} = \frac{C_{11} - C_{12}}{2} \qquad [1]$$

The elastic stiffness matrix of ω-Ti $[C_{ij}]$ can be expressed using these C_{ij} values as follows:

$$[C_{ij}] = \begin{bmatrix} C_{11} & C_{12} & C_{13} & 0 & 0 & 0 \\ C_{12} & C_{11} & C_{13} & 0 & 0 & 0 \\ C_{13} & C_{13} & C_{33} & 0 & 0 & 0 \\ 0 & 0 & 0 & C_{44} & 0 & 0 \\ 0 & 0 & 0 & 0 & C_{44} & 0 \\ 0 & 0 & 0 & 0 & 0 & C_{66} \end{bmatrix}$$

$$= \begin{bmatrix} 196 & 81.2 & 54.5 & 0 & 0 & 0 \\ 81.2 & 196 & 54.5 & 0 & 0 & 0 \\ 54.5 & 54.5 & 249 & 0 & 0 & 0 \\ 0 & 0 & 0 & 54.5 & 0 & 0 \\ 0 & 0 & 0 & 0 & 54.5 & 0 \\ 0 & 0 & 0 & 0 & 0 & 57.2 \end{bmatrix} \qquad [2]$$

The elastic compliance matrix of ω-Ti $[S_{ij}]$ can be converted using a relation of $[S_{ij}] = [C_{ij}]^{-1}$ as follows:

$$[S_{ij}] = \begin{bmatrix} S_{11} & S_{12} & S_{13} & 0 & 0 & 0 \\ S_{12} & S_{11} & S_{13} & 0 & 0 & 0 \\ S_{13} & S_{13} & S_{33} & 0 & 0 & 0 \\ 0 & 0 & 0 & S_{44} & 0 & 0 \\ 0 & 0 & 0 & 0 & S_{44} & 0 \\ 0 & 0 & 0 & 0 & 0 & S_{66} \end{bmatrix}$$

$$= \begin{bmatrix} 0.635 & -0.239 & -0.087 & 0 & 0 & 0 \\ -0.239 & 0.635 & -0.087 & 0 & 0 & 0 \\ -0.087 & -0.087 & 0.439 & 0 & 0 & 0 \\ 0 & 0 & 0 & 1.84 & 0 & 0 \\ 0 & 0 & 0 & 0 & 1.84 & 0 \\ 0 & 0 & 0 & 0 & 0 & 1.75 \end{bmatrix}$$

$$\times \ 10^{-2} \qquad [3]$$

Young's modulus of a hexagonal crystal with an axis perpendicular to the (hkl) plane, E_{hkl}, can be obtained by the following equation[24]:

$$E_{hkl} = \frac{\left\{ h^2 + \frac{(h+2k)^2}{3} + \left(\frac{a_\omega}{c_\omega} l \right)^2 \right\}^2}{S_{11} \left(h^2 + \frac{(h+2k)^2}{3} \right)^2 + S_{33} \left(\frac{a_\omega}{c_\omega} l \right)^4 + (S_{44} + 2 S_{13}) \left(h^2 + \frac{(h+2k)^2}{3} \right) \left(\frac{a_\omega}{c_\omega} l \right)^2} \qquad [4]$$

where a_ω and c_ω represent the lattice constants of ω-Ti. The c_ω/a_ω value of ω-Ti has been reported as ~ 0.61.[25] Therefore, for example, the Young's moduli of ω-Ti with the axes perpendicular to $(0001)_\omega$ and $(11\bar{2}0)_\omega$ or $(10\bar{1}0)_\omega$ are obtained as 228 GPa and 158 GPa, respectively. These values have no meaning as absolute ones because they correspond to the values at 0 K (-273 °C), but they are available as relative ones to discuss the trend of varying Young's modulus with crystallographic orientation in ω-Ti. Equation [4] can be expressed also using the angle between the directions perpendicular to $(0001)_\omega$ and any (hkl) plane Ψ as follows[24]:

$$E_{hkl} = \frac{1}{S_{11} \sin^4 \psi + S_{33} \cos^4 \psi + (S_{44} + 2 S_{13}) \sin^2 \psi \cos^2 \psi} \qquad [5]$$

Figure 6 shows the crystallographic orientation dependence of Young's modulus of ω-Ti on the angle from the direction perpendicular to $(0001)_\omega$. It is found that the Young's moduli of ω-Ti with the axes perpendicular to $(0001)_\omega$ exhibit the maximum level of value. The texture of the ω phase could not be analyzed
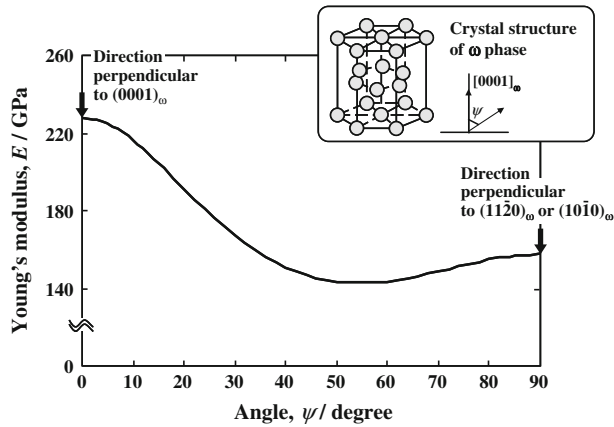
Fig. 6—Crystallographic orientation dependence of Young's modulus of titanium comprising a single ω phase on angle between axes perpendicular to $(0001)_\omega$ and $(11\bar{2}0)_\omega$ or $(10\bar{1}0)_\omega$, calculated using reported elastic stiffness constants of C_{ij}.

Fig. 7—Tensile properties of CR and AT samples.

Fig. 8—Relationship between tensile strength and Young's modulus of TNTZ samples subjected to various thermomechanical treatments.

experimentally using pole figures in XRD and electron backscatter diffraction in SEM because the size and volume fraction of ω phase precipitated in this study are too small to be measured. However, according to the TEM results, the orientation relationship between the β and ω phases can be predicted to be $[111]_\beta // [0001]_\omega$. In the CR and AT samples, the rolling textures of strong $\{001\}_\beta\langle110\rangle_\beta$ and weak $\{211\}_\beta\langle110\rangle_\beta$ were probably formed as shown in Figure 2. The angle between $[111]_\beta$ and $\langle110\rangle_\beta$ is calculated to be 35 deg or 90 deg. Namely, the rolling direction is considered to be preferentially oriented parallel to the direction, which is tilted at 35 deg or 90 deg to $[0001]_\omega$, in the AT samples in this study. Therefore, the Young's modulus of AT samples is not likely to be increased by ω-phase precipitation during aging treatment, resulting in the Young's modulus of AT3.6 sample still almost equal to that of ST sample. However, a quantitative estimation of Young's modulus could not be conducted because the volume fraction of ω phase could not be measured accurately by the limited resolution of TEM in this study.

Figure 7 shows the tensile properties of the CR and AT samples. The tensile properties do not change much for aging times up to 1.8 ks. However, the tensile strength starts to increase for aging times longer than 1.8 ks. The 0.2 pct proof stress also increase, but the elongation decreases for aging times longer than 3.6 ks. A certain elongation is retained after the aging treatment for 10.8 ks. According to the TEM results (Figure 3), one variant of the ω phase was precipitated preferentially in the AT samples subjected to aging treatment for up to 10.8 ks. This result implies that a certain level of ductility may be maintained while one ω-phase variant formation is dominated during aging treatment. At an aging time of 86.4 ks, the tensile strength increases even more, but the elongation becomes almost zero, and as a result, the 0.2 pct proof stress cannot be measured. An aging time of 86.4 ks is therefore unacceptable because a certain level of ductility is required in structural materials for biomedical applications.
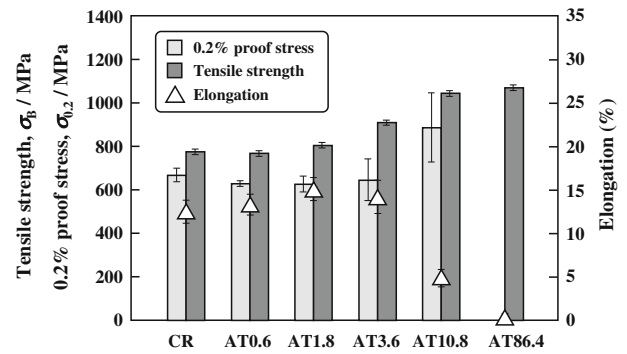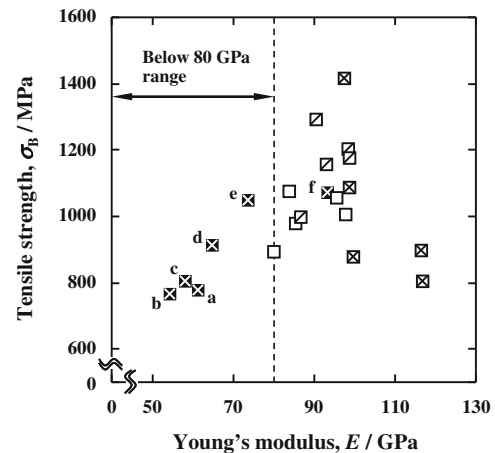
Figure 8 shows the relationship between tensile strength and Young's modulus of the TNTZ samples subjected to various thermomechanical treatments; the data obtained in the current and in previous studies[6–9,11] are included. Previous data showed Young's moduli greater than or equal to 80 GPa. TNTZ samples aged at 573 K or 598 K (300 °C or 325 °C) have much higher Young's moduli (approximately 100 to 120 GPa). Also, their strengths are scattered across a larger range than those of TNTZ samples aged at other temperatures. These effects are the result of the presence of a large amount of ω phase; samples including the ω phase sometimes exhibit much higher strengths (approximately 1400 MPa) when they do not fail in the elastic deformation range during tensile testing. However, in other cases, the brittleness becomes too high to attain plastic deformation during tensile testing, resulting in relatively low tensile strengths (approximately 800 to 900 MPa). In contrast, the AT samples, except AT86.4, had Young's moduli below 80 GPa because of the small amount of crystallographically oriented ω phase formed as a result of the short aging time and rolling texture formation. Among the AT samples, the AT3.6 and

AT10.8 samples exhibit an excellent balance between high strength and low Young's modulus (Figure 8(d) and (e)). Their fatigue properties were therefore examined in this study.

Figure 9 shows the maximum cyclic stress–fatigue life curves (the number of cycles to failure), i.e., S–N curves, of the AT3.6 and AT10.8 samples. In this figure, the fatigue limits of the ST[6,7,9–11] and CR[9] samples, which have been reported previously, are also shown for comparison. The fatigue limit of the AT3.6 sample is similar to those of the ST and CR samples, although the
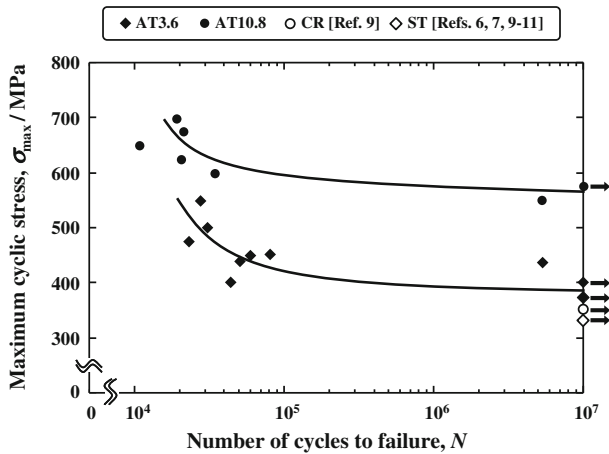
tensile strength of the AT3.6 sample was higher than that of the CR sample, as shown in Figure 7. In the case of the AT10.8 sample, the fatigue limit is increased significantly higher than those of the ST and CR samples.

Figure 10 shows the SEM fractographs of the AT3.6 and AT10.8 samples after fatigue testing at $N > 10^5$ (high-cycle fatigue life region). In both the AT3.6 and AT10.8 samples, a crack-initiation site can be observed near the specimen surface, and the cracks tend to propagate radially from the initiation sites. The fractured surfaces appear ductile, and striations and dimples can be observed; striations with widths of approximately 1.1 μm and 0.8 μm, and dimples with diameters of approximately 3.6 μm and 1.5 μm, can be observed in the stable crack-propagation areas and the fast fracture areas of the AT3.6 and AT10.8 samples, respectively. Both the striation width and the dimple diameter became smaller in the AT10.8 sample than in the AT3.6 sample because of stronger precipitation strengthening. However, in the stable crack-propagation area of the AT10.8 sample, some small cracks can be observed. These results show that some embrittlement occurs by ω-phase precipitation in the AT10.8 sample.

Figure 11 shows the relationship between fatigue limit and Young's modulus of the TNTZ samples subjected to various thermomechanical treatments; the data were obtained in the current and in previous studies.[6–9,11] The AT3.6 sample is classified as being in the low-fatigue-strength group. The AT10.8 sample is at the intermediate level of fatigue strength among the samples,
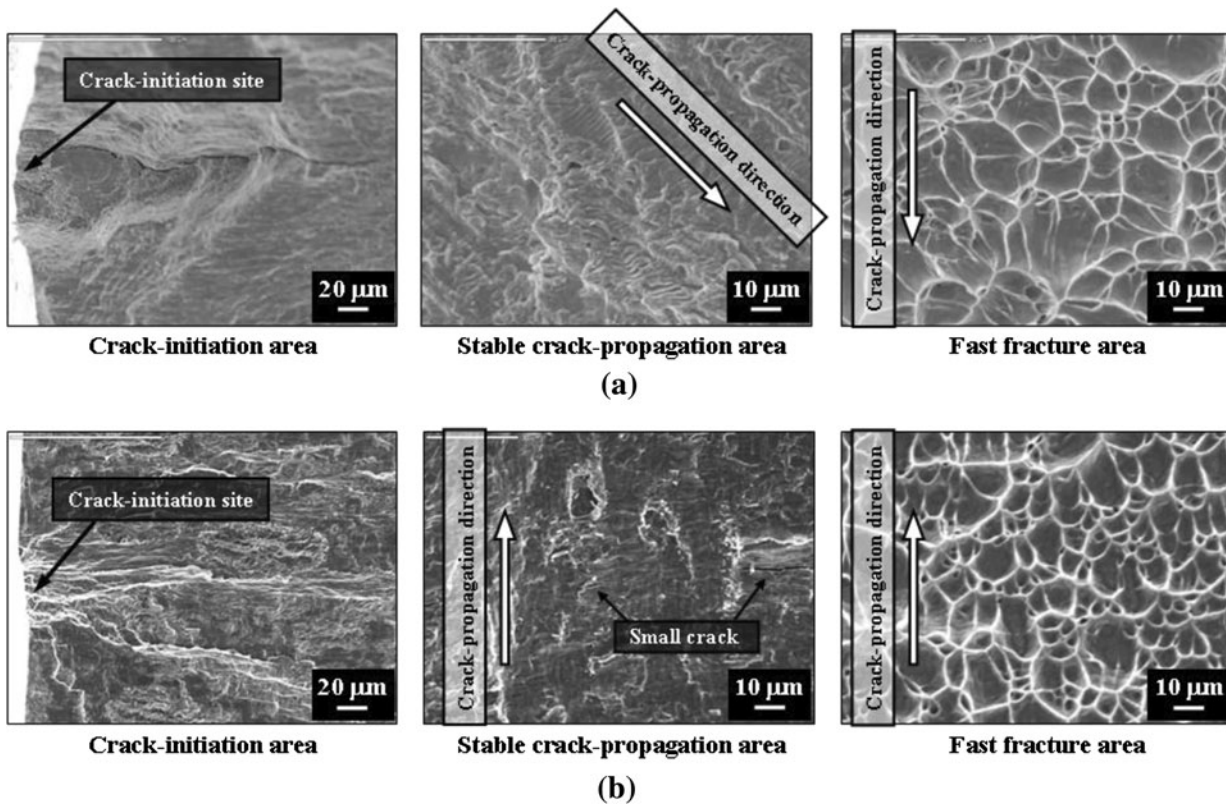

Fig. 9—Fatigue properties of AT3.6 and AT10.8 samples obtained in current study and those of ST and CR samples reported previously.

Fig. 10—SEM fractographs of (a) AT3.6 and (b) AT10.8 samples after fatigue tests (high-cycle fatigue life region: $N > 10^5$).
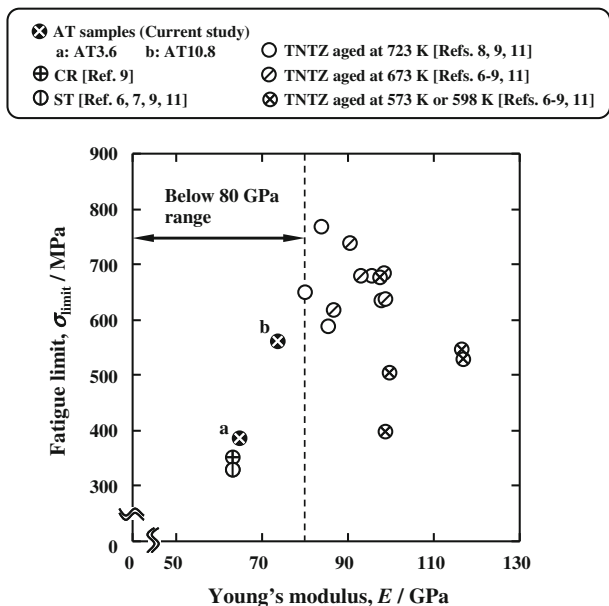
Fig. 11—Relationship between fatigue strength and Young's modulus of TNTZ samples subjected to various thermomechanical treatments.

but it possesses the highest fatigue strength among the samples with a Young's modulus less than 80 GPa (Figure 11(b)). In the case of $\alpha + \beta$-type titanium alloys such as Ti64, the tensile strength and the fatigue strength depend on the texture of primary α phase when the texture is well developed[26]; for example, the tensile strength of Ti64 with the axis parallel to transverse direction is higher than that with the axis parallel to rolling direction because the transverse direction is perpendicular to $(0001)_\alpha$. However, on the contrary, the fatigue strength of Ti64 with the axis parallel to transverse direction is lower than that with the axis parallel to rolling direction.[26,27] The contradiction is caused by the difference of stress conditions between the axes parallel to rolling and transverse directions; the cyclic stress relaxation is difficult to occur in Ti64 with the axis perpendicular to $(0001)_\alpha$. In the case of the ω phase precipitated in this study, $[0001]_\omega$ was not oriented parallel to the rolling direction. Therefore, it is considered that the texture of ω phase is not disadvantageous for improving the fatigue strength of TNTZ.

IV. CONCLUSIONS

To improve the fatigue strength while maintaining a low Young's modulus of a biomedical β-type titanium alloy, Ti–29Nb–13Ta–4.6Zr (TNTZ), a thermomechanical treatment consisting of aging for a short time at an ω-phase-forming temperature of 573 K (300 °C), combined with severe cold rolling, was optimized in this study. The following results were obtained.

1. After solution treatment and cold rolling, TNTZ comprises a single β phase. However, an ω phase starts to precipitate in cold-rolled TNTZ for aging time longer than 0.6 ks
2. The Young's modulus of TNTZ is decreased at once as a pretransitional phenomenon from the β phase to the ω phase by aging. The Young's modulus remains relatively low at an early stage of aging because the amount of the ω phase is small, and as such, the ω phase is oriented preferentially to a direction that is effective for inhibiting the increase in the Young's modulus.
3. The tensile strength can be improved, but the fatigue strength is not changed by aging treatment for 3.6 ks in cold-rolled TNTZ. However, both these strengths can be improved by aging treatment for 10.8 ks. The fatigue strength of TNTZ aged for 10.8 ks after cold rolling exhibits the highest among the values in the range of Young's moduli less than 80 GPa, which is reported in the current and previous studies.
4. The fatigue strength of TNTZ is possibly improved while maintaining relatively low Young's modulus by optimizing ω phase precipitation through aging treatment combined with cold rolling.

REFERENCES

1. M. Niinomi: *J. Mech. Behav. Biomed. Mater.*, 2008, vol. 1, pp. 30–42.
2. J.Y. Rho, T.Y. Tsui, and G.M. Pharr: *Biomaterials*, 1997, vol. 18, pp. 1325–30.
3. P. Zioupos and J.D. Currey: *Bone*, 1998, vol. 22, pp. 57–66.
4. N. Sumitomo, K. Noritake, T. Hattori, K. Morikawa, S. Niwa, K. Sato, and M. Niinomi: *J. Mater. Sci. Mater. Med.*, 2008, vol. 19, pp. 1581–86.
5. D. Kuroda, M. Niinomi, M. Morinaga, Y. Kato, and T. Yashiro: *Mater. Sci. Eng. A*, 1998, vol. 243, pp. 244–49.
6. M. Niinomi, T. Hattori, K. Morikawa, T. Kasuga, A. Suzuki, H. Fukui, and S. Niwa: *Mater. Trans.*, 2002, vol. 43, pp. 2970–77.
7. M. Niinomi: *Biomaterials*, 2003, vol. 24, pp. 2673–83.
8. T. Akahori, M. Niinomi, K. Ishimizu, H. Fukui, and A. Suzuki: *J. Jpn. Inst. Met.*, 2003, vol. 67, pp. 652–60.
9. T. Akahori, M. Niinomi, H. Fukui, M. Ogawa, and H. Toda: *Mater. Sci. Eng. C*, 2005, vol. 25, pp. 248–54.
10. T. Akahori, M. Niinomi, A. Noda, H. Toda, H. Hukui, and M. Ogawa: *J. Jpn. Inst. Met.*, 2006, vol. 70, pp. 295–303.
11. A. Noda: Master's Thesis, Toyohashi University of Technology, Toyohashi, Japan, 2005.

12. T. Furuhara, T. Maki, and T. Makino: *J. Mater. Process. Technol.*, 2001, vol. 117, pp. 318–23.
13. R. Boyer, G. Welsch, and E.W. Collings: *Materials Properties Handbook: Titanium Alloys*, ASM International, Materials Park, OH, 1994.
14. Y.L. Hao, M. Niinomi, D. Kuroda, K. Fukunaga, Y.L. Zhou, R. Yang, and A. Suzuki: *Metall. Mater. Trans. A*, 2002, vol. 33A, pp. 3137–44.
15. Y.L. Hao, M. Niinomi, D. Kuroda, K. Fukunaga, Y.L. Zhou, R. Yang, and A. Suzuki: *Metall. Mater. Trans. A*, 2003, vol. 34A, pp. 1007–12.
16. M. Nakai, M. Niinomi, T. Akahori, H. Tsutsumi, X. Feng, and M. Ogawa: *Mater. Trans.*, 2009, vol. 50, pp. 423–26.
17. T. Akahori, M. Niinomi, M. Nakai, and H. Tsutsumi: *J. Biomech. Sci. Eng.*, 2009, vol. 4, pp. 345–55.
18. M. Tane, S. Akita, T. Nakano, K. Hagihara, Y. Umakoshi, M. Niinomi, and H. Nakajima: *Acta Mater.*, 2008, vol. 56, pp. 2856–63.
19. H. Matsumoto, S. Watanabe, and S. Hanada: *Mater. Trans.*, 2005, vol. 46, pp. 1070–78.
20. T. Inamura, H. Hosoda, K. Wakeshima, and S. Miyazaki: *Mater. Trans.*, 2005, vol. 46, pp. 1597–1603.
21. M. Nakai, M. Niinomi, T. Akahori, and H. Tsutsumi: *Mater. Sci. Forum*, 2010, vols. 654–656, pp. 2134–37.
22. Y.J. Hao, J. Zhu, L. Zhang, J.Y. Qu, and H.S. Ren: *Solid State Sci.*, 2010, vol. 12, pp. 1473–79.
23. J.C. Jamieson: *Science*, 1963, vol. 140, pp. 72–73.
24. J.M. Zhang, Y. Zhang, K.W. Xu, and V. Ji: *Thin Solid Films*, 2007, vol. 515, pp. 7020–24.
25. S.K. Sikka, Y.K. Vohra, and R. Chidambaram: *Progr. Mater. Sci.*, 1982, vol. 27, pp. 245–310.
26. M.R. Bache and W.J. Evans: *Mater. Sci. Eng. A*, 2001, vol. 319, pp. 409–14.
27. W.J. Evans, J.P. Jones, and M.T. Whittaker: *Int. J. Fatigue*, 2005, vol. 27, pp. 1244–50.